

Hydrophobic hydration from small to large lengthscales: Understanding and manipulating the crossover

Sowmianarayanan Rajamani*, Thomas M. Truskett[†], and Shekhar Gardes**

*The Howard P. Isermann Department of Chemical and Biological Engineering and Center for Biotechnology and Interdisciplinary Studies, Rensselaer Polytechnic Institute, Troy, NY 12180; and [†]Department of Chemical Engineering and Institute for Theoretical Chemistry, University of Texas, Austin, TX 78712

Communicated by David Chandler, University of California, Berkeley, CA, May 19, 2005 (received for review February 12, 2005)

Small and large hydrophobic solutes exhibit remarkably different hydration thermodynamics. Small solutes are accommodated in water with minor perturbations to water structure, and their hydration is captured accurately by theories that describe density fluctuations in pure water. In contrast, hydration of large solutes is accompanied by dewetting of their surfaces and requires a macroscopic thermodynamic description. A unified theoretical description of these lengthscale dependencies was presented by Lum, Chandler, and Weeks [(1999) *J. Phys. Chem. B* 103, 4570–4577]. Here, we use molecular simulations to study lengthscale-dependent hydrophobic hydration under various thermodynamic conditions. We show that the hydration of small and large solutes displays disparate dependencies on thermodynamic variables, including pressure, temperature, and additive concentration. Understanding these dependencies allows manipulation of the small-to-large crossover lengthscale, which is nanoscopic under ambient conditions. Specifically, applying hydrostatic tension or adding ethanol decreases the crossover length to molecular sizes, making it accessible to atomistic simulations. With detailed temperature-dependent studies, we further demonstrate that hydration thermodynamics changes gradually from entropic to enthalpic near the crossover. The nanoscopic lengthscale of the crossover and its sensitivity to thermodynamic variables imply that quantitative modeling of biomolecular self-assembly in aqueous solutions requires elements of both molecular and macroscopic hydration physics. We also show that the small-to-large crossover is directly related to the Egelstaff-Widom lengthscale, the product of surface tension and isothermal compressibility, which is another fundamental lengthscale in liquids.

molecular dynamics | salt and additive effects | density fluctuations | nonpolar solvation

Biological self-assembly processes in aqueous solutions are driven by water-mediated interactions between constituents taking part in the assembly. Of these, hydrophobic interactions have received particular attention because of their relevance to protein folding and interactions, micelle and membrane formation, and molecular recognition (1–5). Theoretical work in this direction has been focused on the modeling of primitive hydrophobic phenomena, such as hydration and association of small hydrophobic particles in water (6–13). However, biological assembly occurs over a spectrum of lengthscales from that of an amino acid to proteins and larger. Naturally, fundamental understanding of the lengthscale dependence of hydration and association of hydrophobic solutes in water will be relevant to the quantitative modeling of realistic macromolecular processes (14, 15).

Small hydrophobic solutes can be accommodated into the open hydrogen-bonded network of liquid water without significant perturbations. Indeed, theories that model density fluctuations over small lengthscales in pure water provide a quantitative description of the hydration thermodynamics of small hard-sphere solutes in water (11, 12, 16–18). As the solute size

is increased, water dewets the solute surface. Near a sufficiently large solute, the solute-water interface resembles that between vapor and liquid water, and therefore, requires interfacial thermodynamics for its description (15, 19, 20). Correspondingly, the thermodynamics of hydration changes gradually from entropic for small solutes to enthalpic for large solutes (1, 15). The theoretical approach by Lum, Chandler, and Weeks (LCW) (14) provided a quantitative description of structural and thermodynamic aspects of hydrophobic hydration over the entire small-to-large lengthscale region.

Applications of LCW theory have highlighted the importance of including lengthscales larger than molecular in the description of hydration thermodynamics. For example, the blurring of the entropy convergence in thermal unfolding of proteins (21), the drying-induced collapse of hydrophobic polymers (22), or the strong association of nanoscopic solutes in water cannot be explained based on the physics of small-solute hydration alone. Independent molecular simulation studies of various model nanoscopic solutes in water have also reported dewetting of solute surfaces and the resultant strong water-mediated interactions between those solutes (20, 23–27).

LCW theory predicts that the free energy of hydration of hard-sphere solutes increases approximately linearly with solute volume for small solutes, and with solute surface area for large solutes, and the small-to-large crossover occurs over nanoscopic lengthscales (28). The small-solute hydration is governed by microscopic density fluctuations (11, 12, 16–18), whereas large-solute hydration is described by the thermodynamics of interface formation (1, 15, 19). These two fundamentally different mechanisms will display different dependencies on thermodynamic conditions, thereby providing a mechanism for manipulation of the crossover lengthscale and the associated driving forces.

Motivated by the LCW work (14), here we use molecular dynamics (MD) simulations to probe the lengthscale-dependent hydrophobic hydration as a function of different thermodynamic conditions. Specifically, we focus on hydrophobic hydration in water under tension and in aqueous salt and ethanol solutions. Collectively, our simulation studies confirm the physical picture of lengthscale-dependent hydrophobic hydration presented by the LCW theory and extend that picture in the space of thermodynamic conditions. Specifically, we show that application of tension to water or addition of ethanol brings the small-to-large crossover down to molecular lengthscales, where it can be studied in detail by molecular simulations. By performing temperature-dependent studies under these conditions, we track the gradual transition with solute size from entropy-dominated to enthalpy-dominated hydration thermodynamics. Our simulation studies of alcohol and salt solutions provide

Abbreviations: LCW, Lum, Chandler, and Weeks; MD, molecular dynamics.

[†]To whom correspondence should be addressed. E-mail: gardes@rpi.edu.

© 2005 by The National Academy of Sciences of the USA

quantitative clues to how additives can be expected to impact the small-to-large crossover lengthscale in hydrophobic hydration and the driving forces for hydrophobic aggregation. Finally, we relate the small-to-large crossover to the Egelstaff-Widom lengthscale (29), which is another fundamental lengthscale in liquids.

Methods

MD simulations were performed to calculate the free energy of hydration of hard-sphere solutes with water exclusion radius, R , in the range of 0 to 0.73 nm. Simulations were carried out in the isothermal-isobaric ensemble by using GROMACS (30, 31). Berendsen's barostat and thermostat were used to maintain constant temperature and pressure (32) with coupling time constants of 0.1 ps. The extended simple point charge model (33) was used to represent water molecules explicitly. Periodic boundary conditions were applied, and the particle mesh Ewald method was used to calculate the electrostatic interactions with a grid spacing of 0.12 nm and a cutoff distance of 1 nm. A time step of 2 fs was used in all simulations.

Hydration free energy of small hard-sphere solutes ($R \leq 0.4$ nm) was calculated by using Widom's test particle insertion method from pure water simulations (34, 35). To calculate the hydration free energy of larger hard-sphere solutes, we included a soft-sphere repulsive solute (acting as a biasing potential) interacting with water molecules with energy, R_0^6/r^6 , in the MD simulations. A range of R_0 values from 0.05 to 0.80 nm (in increments of 0.05 nm) was used in a set of simulations that included between 500 and 2,174 extended simple point charge water molecules. Each simulation was equilibrated for 1 ns followed by 4 ns of production run. Configurations (saved every 0.5 ps) obtained from the MD simulations containing the biasing potential were used to evaluate the hydration free energy as a function of the hard-sphere solute radius over small (≈ 1 Å) windows by using perturbation theory (36). These data were combined by minimizing the least-square difference in free energies in the overlapping regions to construct the $\Delta G(R)$ curve.

To obtain the dependence of $\Delta G(R)$ on thermodynamic conditions, we performed free energy calculations in systems under hydrostatic tension. Independent simulations of pure water were performed for three different system sizes to obtain an estimate of the spinodal pressure and density as described in *Results and Discussion*. Calculation of $\Delta G(R)$ at negative pressure requires simulation of metastable systems containing biasing solutes. The presence of such a void in the system can help nucleate phase separation over short time scales used in the simulation. This phenomenon restricts the size of the largest solute that can be simulated as well as the lowest pressure that can be applied. We performed calculations of $\Delta G(R)$ down to pressure as low as $-1,000$ atm (1 atm = 101.3 kPa) for R as large as 0.7 nm.

We also performed calculations of $\Delta G(R)$ at 300 K and 1 atm in ethanol-water mixtures and in sodium chloride solutions at two different concentrations each. Sodium and chloride ions were represented as spherical Lennard-Jones solutes with a unit electronic charge placed at their centers (37). The united-atom representation (38) was used to model ethanol molecules.

Entropic and enthalpic contributions to the free energy were calculated by taking temperature derivatives of the free energy values (39). To that end, we performed calculations of $\Delta G(R)$ at four different temperatures (280, 300, 310, and 320 K) at pressures of 1 atm and $-1,000$ atm (under tension) and in 40 mol% ethanol solution.

Results and Discussion

Fig. 1a shows the hydration free energy of hard-sphere solutes, $\Delta G(R)$, calculated from MD simulations. The hydration free

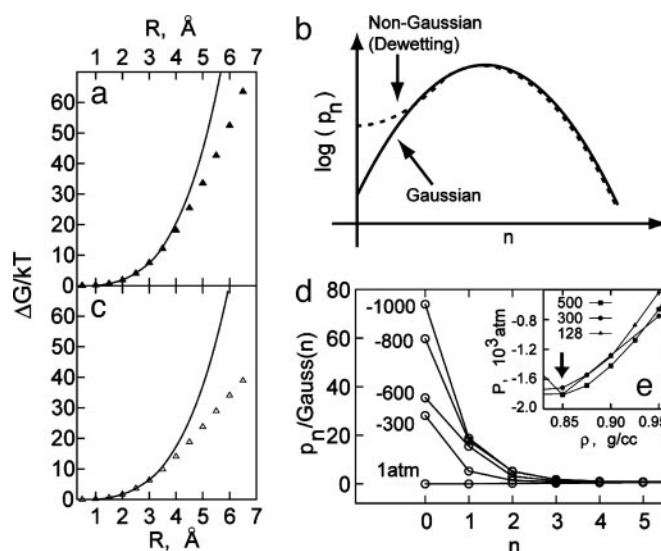


Fig. 1. Density fluctuations and hydration free energy. (a and c) The free energy of formation of a cavity of radius R in water at 1 atm (a) and $-1,000$ atm (c) at 300 K, obtained from MD simulations (triangles) and predicted by using Gaussian theory (lines). (b) A schematic illustration of the Gaussian and non-Gaussian character of density fluctuations. (d) Shown is the ratio, $p_n/\text{Gauss}(n)$, of probabilities measured in MD simulations of pure water and its Gaussian prediction for $R = 4.0$ Å as a function of the applied tension at 300 K. (e) The P - ρ phase diagram of extended simple point charge water at 300 K in the negative pressure region for three different system sizes containing 128, 300, and 500 water molecules.

energy is related to the probability of spontaneous formation of a solute-sized cavity in water, p_0 , by $\Delta G = -kT \ln p_0$ (40). If particle number density fluctuations in a solute-sized observation volume, V , in pure water are approximately Gaussian (17), then

$$\Delta G \approx \frac{kT\rho^2 V^2}{2\sigma^2} + \frac{1}{2} kT \ln(2\pi\sigma^2), \quad [1]$$

where k is the Boltzmann constant, T the temperature, ρ the water number density, and σ^2 the variance of water number in V . Fig. 1a compares $\Delta G(R)$ predicted by Gaussian theory (16) with that obtained from MD simulations under ambient conditions. For small solutes with water exclusion radius $R < 4$ Å, the Gaussian theory predictions are in excellent agreement with the simulation data. Correspondingly, the probability distribution, p_n , of observing exactly n water molecules within a solute-sized observation volume in water is nearly Gaussian (11, 16) for $R < 4$ Å. With increasing solute size, the Gaussian predictions diverge from the measured ΔG values. Indeed, for solutes with $R = 6.0$ Å, Gaussian theory overestimates ΔG by as much as $30 kT$. The onset of discrepancy between Gaussian predictions and MD measurements characterizes the beginning of the small-to-large lengthscale crossover in hydrophobic hydration. The origin of this discrepancy lies in the fundamentally disparate character of large-solute hydration, with

$$\Delta G = \gamma A + PV, \quad [2]$$

where γ is the solute-water surface tension, A the solute surface area, and P the pressure. Huang and Chandler (41) have shown that the above discrepancy is reflected microscopically in the non-Gaussian nature of density fluctuations in the tails of p_n for large V (Fig. 1b), leading to a higher probability of cavity formation that is accompanied by dewetting or drying of the solute surface (14, 19, 20). The different physical mechanisms

underlying small- and large-solute hydration are expected to display different sensitivities to changes in thermodynamic conditions. For example, the entropy of hydration, which characterizes the temperature dependence of free energy, is negative for small solutes and positive for sufficiently large solutes. Similarly, other thermodynamic perturbations can change the hydration free energies of small and large solutes to different extents such that the small-to-large lengthscale crossover can be manipulated in a predictable way, from molecular to nanoscopic lengthscales. In the case of the former, as we demonstrate below, the thermodynamic character of the crossover can be studied through atomistic simulations.

We begin by exploring hydrophobic hydration in the metastable ($P < 0$) region of water's phase diagram (42), which presents unique advantages. The strongly associating nature of water allows the liquid phase to withstand large tensions. Experimental studies on water inclusions in quartz crystals (43, 44), computer simulations (45), and model equations of state (46, 47) predict the spinodal pressure at 300 K to be in the range of $-1,500$ to $-2,000$ atm. By performing simulations of pure extended simple point charge water systems at 300 K in the stretched water region and fitting a polynomial to the $P(\rho)$ curve, we estimate the spinodal pressure to be approximately $-1,780$ atm (Fig. 1e). As expected (48), with increasing tension, cavity formation becomes easier and ΔG values are lowered. Interestingly, Fig. 1c shows that compared with 1 atm at $-1,000$ atm Gaussian theory predicts ΔG accurately over a smaller range of solute sizes ($R < 3.0$ Å). Correspondingly, the density fluctuations become significantly non-Gaussian over molecular lengthscales. Indeed, the actual probability of formation of a 4-Å cavity at $-1,000$ atm is ≈ 80 times larger than its Gaussian prediction, leading to a 10 kJ/mol overestimate of ΔG by the Gaussian theory (Fig. 1d).

The small-to-large lengthscale transition in hydrophobic hydration is better illustrated by plotting the hydration free energy per unit solute surface area, $\Delta G/A$, as a function of solute size (Fig. 2a). In the small-solute region, $\Delta G/A$ increases approximately linearly with the solute size, indicating that the free energy scales approximately linearly with the solute volume in this region. With increasing solute size, the $\Delta G/A$ profile becomes sublinear and is in quantitative agreement with previous calculations (28). These data can be extrapolated by using $\Delta G/A = \gamma(R) + PR/3$, consistent with a gradual transition to interfacial thermodynamics with increasing solute size (Fig. 2c). The curvature dependence of γ is captured approximately by $\gamma(R) = \gamma_\infty(1 - 2\delta/R)$, where δ is the Tolman length, and $\gamma_\infty = \lim_{R \rightarrow \infty} \gamma(R)$. We use $\gamma_\infty = 73.6$ dynes/cm and $\delta = 0.76$ Å as in ref. 28.

The asymptotic approach to the macroscopic thermodynamic description with increasing solute size is consistent with the contact density profiles (19, 24) (Fig. 2b). For small solutes, the density of water in contact with the solute, $g(R)$, increases with R and reaches a maximum for solutes with $2 < R < 2.5$ Å (49). Increasing the solute size further leads to growth of the void volume and a corresponding loss of favorable enthalpic interactions by vicinal water molecules characterized by Hummer and Garde (20) in terms of the "cavity expulsion" potential. That loss results in a gradual dewetting of hydrophobic solutes with increasing solute size. For sufficiently large solutes, $g(R)$ varies inversely with R and its numerical value drops well below the bulk density of water (19). In this limit, the solute-water interface resembles the interface between vapor and liquid water, and therefore, surface tension dominated hydration behavior is expected (1, 15, 19).

The small-to-large crossover lengthscale characterizes the size at which macroscopic hydration thermodynamics also becomes relevant. The point of intersection of the Gaussian theory line ($\Delta G/A$ from Eq. 1) and the $\gamma_\infty(1 - 2\delta/R) + PR/3$ curve provides an approximate measure of that lengthscale.

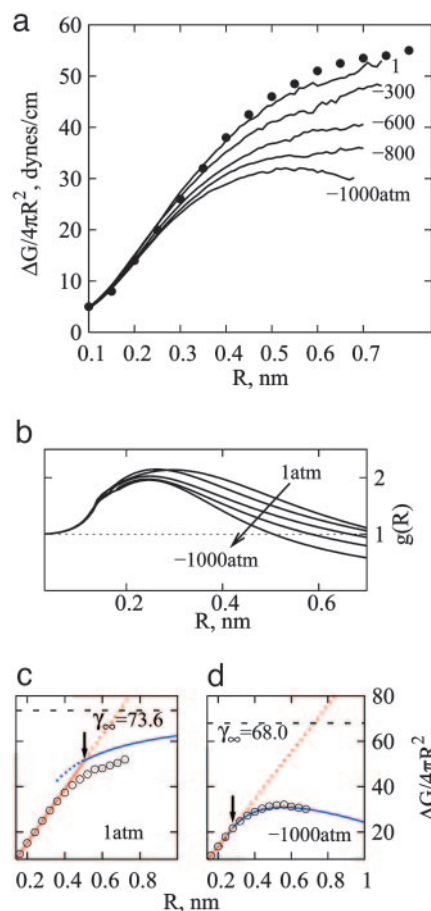


Fig. 2. Crossover lengthscale in hydrophobic hydration. (a) The free energy of hydration of a hard-sphere solute per unit surface area, $\Delta G/4\pi R^2$, as a function of the exclusion radius, R , at 300 K was obtained from MD simulations at different tensions. Independent results from Huang *et al.* (28) at 1 atm are also shown (●). (b) The contact density of water relative to its bulk density as a function of R at five different tensions is shown. The curves are Padé fits to $g(R)$ data calculated from ΔG values (49). (c and d) Shown are $\Delta G/A$ curves at 1 atm (c) and $-1,000$ atm (d) along with linear fits to Gaussian theory prediction in the small-solute region (red) and the $\gamma_\infty(1 - 2\delta/R) + PR/3$ curve in the large-solute limit (blue). We calculated the dependence of γ_∞ on tension by using a molecular thermodynamic theory for water (50): γ_∞ equals 73.6 dynes/cm at 1 atm and reduces to 68 dynes/cm at $-1,000$ atm, shown by horizontal dashed lines. $\delta = 0.76$ Å (28) is assumed to be a constant. Arrows indicate the crossover length as the point of intersection of small- and large-solute hydration behavior.

The crossover length calculated by using this definition is rather small (subnanoscopic) under ambient conditions, equal to ≈ 5 Å, which is followed by a broad transition region in the $\Delta G/A$ profile. With increasing tension, although the $\Delta G/A$ profile remains qualitatively similar, the crossover region shifts to even smaller lengthscales (≈ 3 Å). Why does the crossover length decrease with increasing tension? The answer lies in the characteristically different dependence of ΔG on pressure (tension) for small and large solutes, implied by Eqs. 1 and 2, respectively. With increasing tension, at 300 K, ρ decreases (Fig. 1e) and σ^2 increases slightly, leading to the lowering of $\Delta G/A$ values for small solutes. For large solutes, the decrease in $\Delta G/A$ with increasing tension arises directly from the PV term, and indirectly through the γA term. To our knowledge, no direct measurements of γ have been reported in metastable water. However, an approximately linear dependence of γ on ρ is expected (50). At $-1,000$ atm, the PV term for interme-

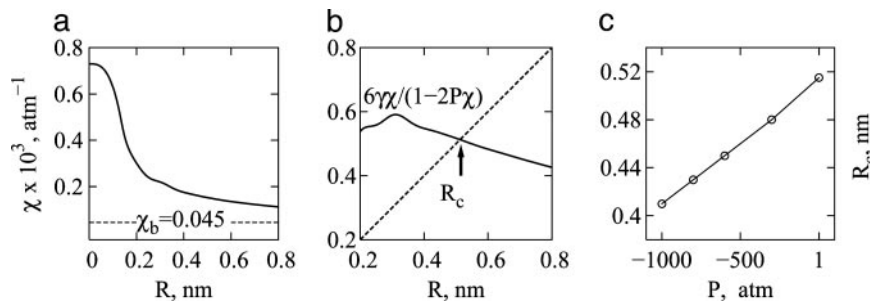


Fig. 3. Prediction of the crossover lengthscale and its connection to the Egelstaff–Widom lengthscale. (a) The microscopic compressibility, $\chi = \sigma^2/kT\rho^2V$, as a function of the radius of spherical observation volumes calculated from MD simulations at 300 K and 1 atm is shown. The dashed line denotes the bulk water isothermal compressibility, $\chi_b = 4.5 \times 10^{-5} \text{ atm}^{-1}$. (b) A graphical solution of Eq. 3, obtained as a point of intersection of the curve $y = 6\gamma\chi/(1 - 2P\chi)$ (solid line) and $y = R$ (dashed line). We used $\chi(R)$ from a and $\gamma(R) = \gamma_\infty(1 - 2\delta/R)$. (c) The values of R_c predicted by solving Eq. 3 as a function of the applied tension are shown.

diate-sized solutes becomes comparable to the γA term, leading to the negative slope of $\Delta G/A$ line for larger solutes (Fig. 2d).

A simple thermodynamic argument provides a basis for the disparate pressure dependencies discussed above. The pressure derivative of $\Delta G/A$ is proportional to the solute size:

$$\left[\frac{\partial(\Delta G/A)}{\partial P} \right]_T = \frac{\Delta V}{A} \propto R,$$

where ΔV is the excess volume of hydration of the solute (51). Thus, the decrease in $\Delta G/A$ is smaller for molecular solutes compared with that for larger solutes, effectively reducing the crossover length with increasing tension.

The crossover lengthscale characterizes the region where small and large lengthscale hydration descriptions overlap. Indeed, equating Eqs. 1 and 2 [i.e., $kT\rho^2V^2/2\sigma^2 + 1/2kT\ln(2\pi\sigma^2) = \gamma A + PV$] and neglecting the logarithmic term on the left side of the equation, we get the crossover length scale

$$R_c \approx \frac{6\gamma\chi}{1 - 2P\chi}, \quad [3]$$

where $\chi = \sigma^2/kT\rho^2V$ is the microscopic compressibility. Both the surface tension and the microscopic compressibility depend on R , and therefore, values of γ and χ at $R = R_c$ need to be used in Eq. 3. The curvature dependence of γ is given approximately by the Tolman equation (see Fig. 2c). Fig. 3a shows the R dependence of the microscopic compressibility obtained from computer simulations. For molecular volumes, χ is ≈ 5 –10 times larger than the bulk water compressibility, χ_b , and decreases monotonically to χ_b in the thermodynamic limit. Egelstaff and Widom (29) found that, although individual values of γ_∞ and χ_b for a range of liquids vary by a factor of 150, the product $\gamma_\infty\chi_b$ remains almost constant equal to a few tenths of an angstrom ($\gamma_\infty\chi_b \approx 0.34 \text{ \AA}$ for water). Thus, Eq. 3 suggests a remarkable relationship between the crossover lengthscale and the Egelstaff–Widom lengthscale, $\gamma_\infty\chi_b$, a fundamental length characteristic of liquids.

A graphical solution of Eq. 3 provides the value of the crossover length, R_c , which is subnanoscopic (Fig. 3b). In addition, the pressure dependence of R_c predicted by Eq. 3 is consistent with our earlier observations. Specifically, application of tension reduces the crossover length to molecular sizes (Fig. 3c). The fact that the crossover length is related to the Egelstaff–Widom lengthscale is physically intuitive, because the latter quantity contains information about both molecular (χ) and macroscopic (γ) solvation physics.

Does the reduction in crossover length imply a similar transition in the thermodynamic nature of hydrophobic hydration

with increasing tension? The entropic ($-T\Delta S$) and enthalpic (ΔH) contributions to ΔG calculated by taking temperature derivatives of ΔG are shown in Fig. 4. Although the calculated entropy and enthalpy values contain significant statistical uncertainties, at 1 atm, entropy makes the major contribution to the free energy over the entire solute size range considered here. In contrast, at $-1,000$ atm, entropy dominates over a significantly smaller range of solute sizes ($R < 3 \text{ \AA}$), with the hydration of larger solutes being predominantly enthalpic in nature. Because surface tension decreases monotonically with temperature, the entropy of hydration of sufficiently large solutes is expected to be positive (favorable). However, at $-1,000$ atm, the entropy of hydration of larger solutes remains small but negative (unfavorable), suggesting that crossover to large-solute hydration is not complete over the range of solute sizes studied here. That is, the region of crossover from small-to-large-solute hydration is broad, and the crossover size simply characterizes a lengthscale at which elements of large-solute hydration physics also become important.

The sign of the hydration enthalpy determines the temperature dependence of the solubility as well. Nonpolar gases display a minimum in their aqueous solubility with increasing temperature. The hydration enthalpy becomes positive above the solubility minimum temperature (52, 53). For small hard-sphere solutes, Gaussian theory (54) as well as the exact point-particle limit of the scaled particle theory (55) indicate that the sign of the hydration enthalpy is positive above the temperature of maximum density (TMD) of liquid water.

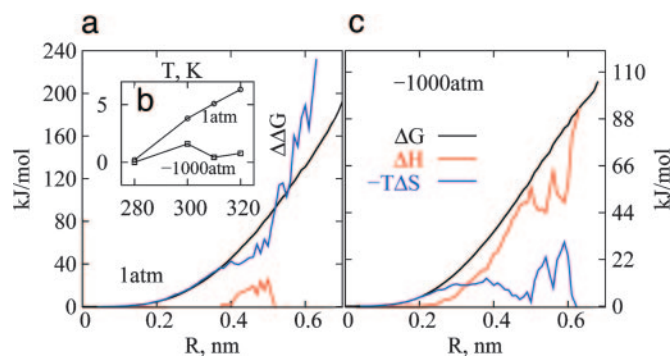


Fig. 4. Thermodynamics of small and large solute hydration. (a and c) The hydration free energy of a hard-sphere solute, ΔG , as a function of solute size R , at 1 atm (a) and $-1,000$ atm (c) at 300 K. (b) The temperature dependence of ΔG is shown with reference to its value at 280 K [$\Delta\Delta G = \Delta G(T) - \Delta G(280\text{K})$] for a hard-sphere solute of radius 4.5 \AA . (c) The enthalpic (ΔH , red) and entropic ($-T\Delta S$, blue) contributions to ΔG obtained from temperature derivatives of the free energy are shown at 300 K. Thermodynamic crossover from entropic to enthalpic hydration is clear at $-1,000$ atm.

1. Chandler, D. (2005) *Nature*, in press.
2. Kauzmann, W. (1959) *Adv. Protein Chem.* **14**, 1–63.
3. Tanford, C. (1973) *The Hydrophobic Effect* (Wiley, New York).
4. Dill, K. A. (1990) *Biochemistry* **29**, 7133–7155.
5. Maibaum, L., Dinner, A. R. & Chandler, D. (2004) *J. Phys. Chem. B* **108**, 6778–6781.
6. Pratt, L. R. & Chandler, D. (1977) *J. Chem. Phys.* **67**, 3683–3704.
7. Pangali, C., Rao, M. & Berne, B. J. (1979) *J. Chem. Phys.* **71**, 2975–2981.
8. Smith, D. E. & Haymet, A. D. J. (1993) *J. Chem. Phys.* **98**, 6445–6454.
9. Guillot, B. & Guissani, Y. (1993) *J. Chem. Phys.* **99**, 8075–8094.
10. Lazaridis, T. & Paulaitis, M. E. (1994) *J. Phys. Chem.* **98**, 635–642.
11. Hummer, G., Garde, S., García, A. E., Paulaitis, M. E. & Pratt, L. R. (1998) *J. Phys. Chem. B* **102**, 10469–10482.
12. Hummer, G., Garde, S., García, A. E. & Pratt, L. R. (2000) *Chem. Phys.* **258**, 349–370.
13. Pratt, L. R. (2002) *Annu. Rev. Phys. Chem.* **53**, 409–436.
14. Lum, K., Chandler, D. & Weeks, J. D. (1999) *J. Phys. Chem. B* **103**, 4570–4577.
15. Chandler, D. (2002) *Nature* **417**, 491.
16. Hummer, G., Garde, S., García, A. E., Pohorille, A. & Pratt, L. R. (1996) *Proc. Natl. Acad. Sci. USA* **93**, 8951–8955.
17. Garde, S., Hummer, G., García, A. E., Paulaitis, M. E. & Pratt, L. R. (1996) *Phys. Rev. Lett.* **77**, 4966–4968.
18. Gomez, M. A., Pratt, L. R., Hummer, G. & Garde, S. (1999) *J. Phys. Chem.* **103**, 3520–3523.
19. Stillinger, F. H. (1973) *J. Sol. Chem.* **2**, 141–158.
20. Hummer, G. & Garde, S. (1998) *Phys. Rev. Lett.* **80**, 4193–4196.
21. Huang, D. M. & Chandler, D. (2000) *Proc. Natl. Acad. Sci. USA* **97**, 8324–8327.
22. ten Wolde, P. R. & Chandler, D. (2002) *Proc. Natl. Acad. Sci. USA* **99**, 6539–6543.
23. Wallqvist, A. & Berne, B. J. (1995) *J. Phys. Chem.* **99**, 2893–2899.
24. Ashbaugh, H. S. & Paulaitis, M. E. (2001) *J. Am. Chem. Soc.* **123**, 10721–10728.
25. Huang, X. H., Margulis, C. J. & Berne, B. J. (2003) *Proc. Natl. Acad. Sci. USA* **100**, 11953–11958.
26. Zhou, R. H., Huang, X. H., Margulis, C. J. & Berne, B. J. (2004) *Science* **305**, 1605–1609.
27. Choudhury, N. & Pettitt, B. M. (2005) *J. Am. Chem. Soc.* **127**, 3556–3567.
28. Huang, D. M., Geissler, P. L. & Chandler, D. (2001) *J. Phys. Chem. B* **105**, 6704–6709.
29. Egelstaff, P. A. & Widom, B. (1970) *J. Chem. Phys.* **53**, 2667–2669.
30. Lindahl, E., Hess, B. & van der Spoel, D. (2001) *J. Mol. Mod.* **7**, 306–317.
31. Berendsen, H. J. C., van der Spoel, D. & van Drunen, R. (1995) *Comp. Phys. Commun.* **91**, 43–56.
32. Berendsen, H. J. C., Postma, J. P. M., van Gunsteren, W. F., DiNola, A. & Haak, J. R. (1984) *J. Chem. Phys.* **81**, 3684–3690.
33. Berendsen, H. J. C., Grigera, J. R. & Straatsma, T. P. (1987) *J. Phys. Chem.* **91**, 6269–6271.
34. Widom, B. (1982) *J. Phys. Chem.* **86**, 869–872.
35. Lee, B. (1985) *J. Chem. Phys.* **83**, 2421–2425.
36. Frenkel, D. & Smit, B. (2002) *Understanding Molecular Simulations* (Academic, San Diego), 2nd Ed.
37. Smith, D. E. & Dang, L. X. (1994) *J. Chem. Phys.* **100**, 3757–3766.
38. Jorgensen, W. L. (1986) *J. Phys. Chem.* **90**, 1276–1284.
39. Ghosh, T., García, A. E. & Garde, S. (2002) *J. Chem. Phys.* **116**, 2480–2486.
40. Pohorille, A. & Pratt, L. R. (1990) *J. Am. Chem. Soc.* **112**, 5066–5074.
41. Huang, D. M. & Chandler, D. (2000) *Phys. Rev. E* **61**, 1501–1506.
42. Debenedetti, P. G. (1996) *Metastable Liquids* (Princeton Univ. Press, Princeton).
43. Green, J. L., Durben, D. J., Wolf, G. H. & Angell, C. A. (1990) *Science* **249**, 649–652.
44. Zheng, Q., Durben, D. J., Wolf, G. H. & Angell, C. A. (1991) *Science* **254**, 829–832.
45. Netz, P. A., Starr, F. W., Stanley, H. E. & Barbosa, M. C. (2001) *J. Chem. Phys.* **115**, 344–347.
46. Speedy, R. J. (1982) *J. Phys. Chem.* **86**, 982–991.
47. Truskett, T. M., Debenedetti, P. G., Sastry, S. & Torquato, S. (1999) *J. Chem. Phys.* **111**, 2647–2656.
48. Punnathanam, S. & Corti, D. S. (2004) *Phys. Rev. E* **69**, 036105-1–036105-8.
49. Pratt, L. R. & Pohorille, A. (1992) *Proc. Natl. Acad. Sci. USA* **89**, 2995–2999.
50. Truskett, T. M., Debenedetti, P. G. & Torquato, S. (2001) *J. Chem. Phys.* **114**, 2401–2418.
51. Ben-Naim, A. (1980) *Hydrophobic Interaction* (Plenum, New York).
52. Preston, G. T., Funk, E. W. & Prausnitz, J. M. (1971) *Phys. Chem. Liq.* **2**, 193–196.
53. Prausnitz, J. M. (1986) *Molecular Thermodynamics of Fluid Phase Equilibria* (Prentice-Hall, Englewood Cliffs, NJ).
54. Garde, S., García, A. E., Pratt, L. R. & Hummer, G. (1999) *Biophys. Chem.* **78**, 21–32.
55. Reiss, H., Frisch, H. L., Helfand, E. & Lebowitz, J. L. (1959) *J. Chem. Phys.* **31**, 369–380.
56. Feeney, M. R. & Debenedetti, P. G. (2003) *Ind. Eng. Chem. Res.* **42**, 6396–6405.
57. Jarvis, N. L. & Scheiman, M. A. (1968) *J. Phys. Chem.* **72**, 74–78.
58. Cioci, F. & Lavecchia, R. (1997) *AIChE J.* **43**, 525–534.
59. Collins, K. D. & Washabaugh, M. W. (1985) *Q. Rev. Biophys.* **4**, 323–422.
60. Collins, K. D. (2004) *Methods* **34**, 300–311.
61. Ashbaugh, H. S. & Pratt, L. R. (2005) *Rev. Mod. Phys.*, arXiv archive, <http://arxiv.org/abs/physics/0307109>.
62. Rossky, P. J. (2001) *Nature* **410**, 645–648.
63. Koishi, T., Yoo, S., Yasuoka, K., Xeng, X. C., Narurni, T., Susukita, R., Kawai, A., Furusawa, H., Suenaga, A., Okimoto, N., *et al.* (2004) *Phys. Rev. Lett.* **93**, 185701-1.
64. Vaitheeswaran, S., Yin, H., Rasaiah, J. C. & Hummer, G. (2004) *Proc. Natl. Acad. Sci. USA* **101**, 17002–17005.